Available online at www.sciencedirect.com
SCIENCE DIRECT®
International Journal of Heat and Mass Transfer 48 (2005) 3128–3139
International Journal of HEAT and MASS TRANSFER
www.elsevier.com/locate/ijhmt

Bifurcated three-dimensional forced convection in plane symmetric sudden expansion

M. Thiruvengadam, J.H. Nie, B.F. Armaly *

Department of Mechanical and Aerospace Engineering, University of Missouri-Rolla, Rolla, MO 65401, United States

Received 25 December 2004; received in revised form 4 February 2005
Available online 20 April 2005

Abstract

Simulations of bifurcated three-dimensional laminar forced convection in horizontal duct with plane symmetric sudden expansion are presented to illustrate the effects of flow bifurcations on temperature and heat transfer distributions. The stable bifurcated flow that develops in this symmetric geometry leads to non-symmetric temperature and heat transfer distributions in the transverse direction, but symmetric distributions with respect to the center width of the duct in the spanwise directions for the Reynolds number of 400–800. A strong downwash develops at the corner of the step and a smaller reverse flow region develops adjacent to the lower stepped wall than the one that develops adjacent to the upper stepped wall. The downwash and the ''jet-like'' flow that develop near the sidewall create a strong swirling spanwise flow in the primary recirculating flow regions downstream from the sudden expansion. The magnitude of maximum Nusselt number that develops on the lower stepped walls is higher than the one that develops on the upper stepped wall. The locations of these maximum Nusselt numbers on the stepped walls are near the sidewalls and are upstream of the ''jet-like'' flow impingement regions. Results reveal that the locations where the streamwise component of wall shear stress is zero on the stepped walls do not coincide with the outer edge of the recirculation flow region near the sidewalls. Velocity, temperature, Nusselt number, and friction coefficient distributions are presented.

1. Introduction

Flow separation and reattachment due to sudden changes in geometry in internal flow occur in many engineering applications where heating or cooling is required. These applications appear in electronic cooling equipment, cooling of turbine blades, combustion chambers, and many other heat exchanging devices. The flow and the heat transfer in most of these applications exhibit three-dimensional (3-D) behavior, but most of the published heat transfer results deals only with the two-dimensional (2-D) behavior. Experimental and numerical studies [1–5] have shown that laminar flow in plane symmetric sudden expansion exhibits symmetric steady laminar flow behavior for Reynolds number lower than a critical value, and asymmetric steady laminar flow behavior for Reynolds number higher than the critical value. Results have also shown that the flow becomes unsteady as the Reynolds number continues to increase.

Fearn et al. [1] presented the measured and predicted results for flow in a duct with an expansion ratio of 3 and downstream aspect ratio of 8 and determined that the critical Reynolds number is 108. They observed a laminar and stable bifurcated flow regime for Reynolds number ranging between 108 and 413, and unsteady

* Corresponding author. Tel.: +1 573 341 4601; fax: +1 573 341 4607.
E-mail address: armaly@umr.edu (B.F. Armaly).

0017-9310/$ - see front matter © 2005 Elsevier Ltd. All rights reserved.
doi:10.1016/j.ijheatmasstransfer.2005.02.019

Nomenclature

AR	upstream aspect ratio = W/h
AR_1	downstream aspect ratio = W/H
C_f	skin friction coefficient = $2\tau_w/\rho u_0^2$
C_p	specific heat
ER	expansion ratio = H/h
H	duct height downstream from the step
h	duct height upstream from the step
k	thermal conductivity
L	half width of the duct
Nu	Nusselt number = $q_w S/k(T_w - T_0)$
q_w	wall heat flux = $-k\partial T/\partial n$ at the wall
Re	Reynolds number = $2\rho u_0 h/\mu$
S	step height
T	temperature
T_0	inlet fluid temperature
u	velocity component in the x-coordinate direction
u_0	average inlet velocity
v	velocity component in the y-coordinate direction
W	width of the duct
w	velocity component in the z-coordinate direction
x	streamwise coordinate
y	transverse coordinate
z	spanwise coordinate
x_b	outer boundary of the primary recirculation region
x_u	locations where the streamwise velocity gradient is zero ($\partial u/\partial y = 0$)
μ	dynamic viscosity
ρ	density
τ_w	wall shear stress = $\mu\sqrt{(\partial u/\partial y)^2 + (\partial w/\partial y)^2}$ on the stepped wall, and $=\mu\sqrt{(\partial u/\partial z)^2 + (\partial v/\partial z)^2}$ on the sidewall

laminar flow regime for Reynolds number higher than 413. Durst et al. [2] measured streamwise velocity distributions for $Re = 75$, 152, and 344 in a duct with an expansion ratio of 3 and downstream aspect ratio of 9.2. This range of Reynolds number covered the laminar symmetric flow regime for $Re = 75$ and the laminar stable bifurcated flow regime for $Re = 152$ and 344. They demonstrated experimentally that the asymmetry can flip flop from one stepped wall to the other due to disturbances in the inlet flow and instabilities that develop in the separated shear layer. Similarly, Durst et al. [3] measured and predicted results for an expansion ratio of 2 and downstream aspect ratio of 8, and established the critical Reynolds number for this geometry to be 167. Cherdron et al. [4] demonstrated experimentally that the critical Reynolds number increases both with decreasing the aspect ratio and the expansion ratio. They reported critical Reynolds numbers as a function of downstream aspect ratio for expansion ratios of 2 and 3. Hawa and Rusak [5] used asymptotic linear instability analyses, and numerical simulations to study in detail the dynamics and the instabilities of the bifurcated 2-D flow in this geometry. Battaglia et al. [6] demonstrated numerically that the critical Reynolds number is a function of the expansion ratio (decreases with increasing expansion ratio), and they established that the convergence time of the numerical solution increases significantly as the critical Reynolds number is approached. Drikakis [7] concluded from numerical studies that the critical Reynolds number decreases with the increase of the expansion ratio and the asymmetry increases with the increase of the Reynolds number. Patel and Drikakis [8] demonstrated numerically that the critical Reynolds number is influenced by the discretization scheme of the advective flux terms that appear in the governing equations and recommended a second or higher order finite difference scheme for accurate simulations. Chiang et al. [9] demonstrated numerically that the critical Reynolds number is a function of the duct's aspect ratio (3-D simulation). They established that for an expansion ratio of 3 and a Reynolds number equal to or smaller than 160, the flow will be symmetric when the upstream aspect ratio is smaller than 3.5. Schreck and Schafer [10] used a parallel multi-grid finite volume solver to simulate 3-D bifurcation in a duct with expansion ratio of 3, and reported critical Reynolds numbers for downstream aspect ratio of 5 and 2. All of the above studies were limited to the isothermal flow case.

Tsui and Shu [11] examined numerically the 2-D laminar mixed convection in an inclined duct with an expansion ratio of 3. The buoyancy assisted flow, with vertical orientation, remained symmetric for $Re \leqslant 75$ and Grashof numbers in the range of 1000–3000 (where the Grashof number is based on the upstream duct height and the walls-inlet flow temperature difference). When the Reynolds number increased to 152 (thus lowering the buoyancy force), the flow field was either symmetric or asymmetric depending on the magnitude of the Grashof number. The buoyancy opposing flow resulted in a wavy non-symmetric structure with several recirculation flow regions that increased the heat transfer. Nie and Armaly [12] examined numerically the three-dimensional forced

convection in a duct with expansion ratio of 2 and upstream aspect ratio of 4, but that study was limited to Reynolds number below the critical value, i.e. symmetric flow regime.

The majority of published results for plane symmetric sudden expansion in a duct have dealt with the isothermal two-dimensional flow case. To the authors' knowledge the only published three-dimensional heat transfer results have been limited to the non-bifurcated flow regime [12]. This fact, along with the realization that such geometry appears regularly in many industrial heat transfer devices, motivated the present study.

2. Problem statement and solution procedure

Three-dimensional laminar forced convection in a horizontal duct with a plane symmetric sudden expansion is simulated, and a schematic of the computational domain is presented in Fig. 1. The duct's heights (H) and (h) downstream and upstream of the expansion respectively are 0.04 m and 0.02 m. The step height (S) and the duct's width (W) are maintained as 0.01 m and 0.08 m, respectively. This geometry provides a configuration with an expansion ratio (ER = H/h) of 2, an upstream aspect ratio (AR = W/h) of 4, and a downstream aspect ratio ($AR_1 = W/H$) of 2. The origin of the coordinate system is located at the bottom corner of the step where the sidewall, the backward-facing step and the lower stepped-wall intersect, as shown in Fig. 1. The directions of the streamwise (x), spanwise (z), and transverse (y) coordinates are shown in that figure. The length of the computational domain is 0.8 m downstream and 0.02 m upstream of the step, respectively, i.e. $-2 \leqslant x/S \leqslant 80$. This choice was made to insure that the flow at the inlet section of the duct ($x/S = -2$) is not affected by the sudden expansion in geometry, and the flow at the exit section of the duct ($x/S = 80$) can be treated as fully developed. It was confirmed that the use of a longer computational domain did not change the flow or the thermal behavior in the region downstream from the step ($x/S < 40$). The three-dimensional steady, and also the transient Navier-Stokes, energy, and continuity equations for laminar incompressible flow are solved numerically using the finite volume method. The physical properties are treated as constants and evaluated for air at the inlet temperature of $T_0 = 20$ °C (i.e., density (ρ) is 1.205 kg/m^3, specific heat (C_p) is 1005 J/kg °C, dynamic viscosity (μ) is 1.81×10^{-5} kg/m s, and thermal conductivity (k) equals to 0.0259 W/m °C). Inlet flow ($x/S = -2$, $1 \leqslant y/S \leqslant 3$, for all z) is considered to be isothermal ($T_0 = 20$ °C), hydrodynamically steady and fully developed with a distribution for the streamwise velocity component (u) equal to the one described by Shah and London [13]. The other velocity components (v and w) are set to be equal to zero at that inlet section. The no-slip boundary condition (zero velocities) is applied to all of the wall surfaces. Uniform and constant wall heat flux ($q_w = 5$ W/m^2) is specified for the stepped walls ($y/S = 0$ and 4, $0 \leqslant x/S \leqslant 80$, for all z), while other walls are treated as adiabatic surfaces. At this low wall heat flux and for this horizontal orientation of the duct, the buoyancy effects can be, and was, neglected in the simulations. Fully developed flow and thermal conditions are imposed at the exit section ($x/S = 80$, for all y and z) of the calculation domain.

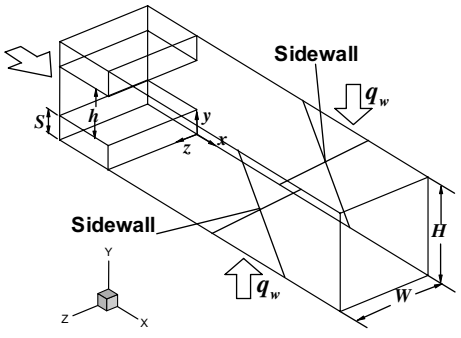

Fig. 1. Schematic of the computational domain.

Numerical solution of the governing equations and boundary conditions was performed by utilizing the commercial computational fluid dynamics (CFD) code FLUENT 6.0. The mesh is generated using FLUENT's preprocessor GAMBIT. Hexahedron volume elements were used in the simulation. At the end of each iteration, the residual sum for each of the conserved variables was computed and stored, thus recording the convergence history. The convergence criterion required that the scaled residuals be smaller than 10^{-10} for the mass and the momentum equations and smaller than 10^{-11} for the energy equation. Calculations were performed on DELL workstations, and the CPU time for converged solution for $Re = 600$ is approximately 24 h. The SIMPLEC algorithm is used for the pressure velocity coupling, and the momentum and energy equations are discretized with the second-order upwind scheme in order to improve the accuracy of the simulations. Detailed descriptions of the CFD code and the solution procedures may be found in the FLUENT manual.

3. Code and model validations

Numerical simulations of the velocity and temperature distribution in this geometry revealed a symmetric behavior relative to the center width of the duct as can

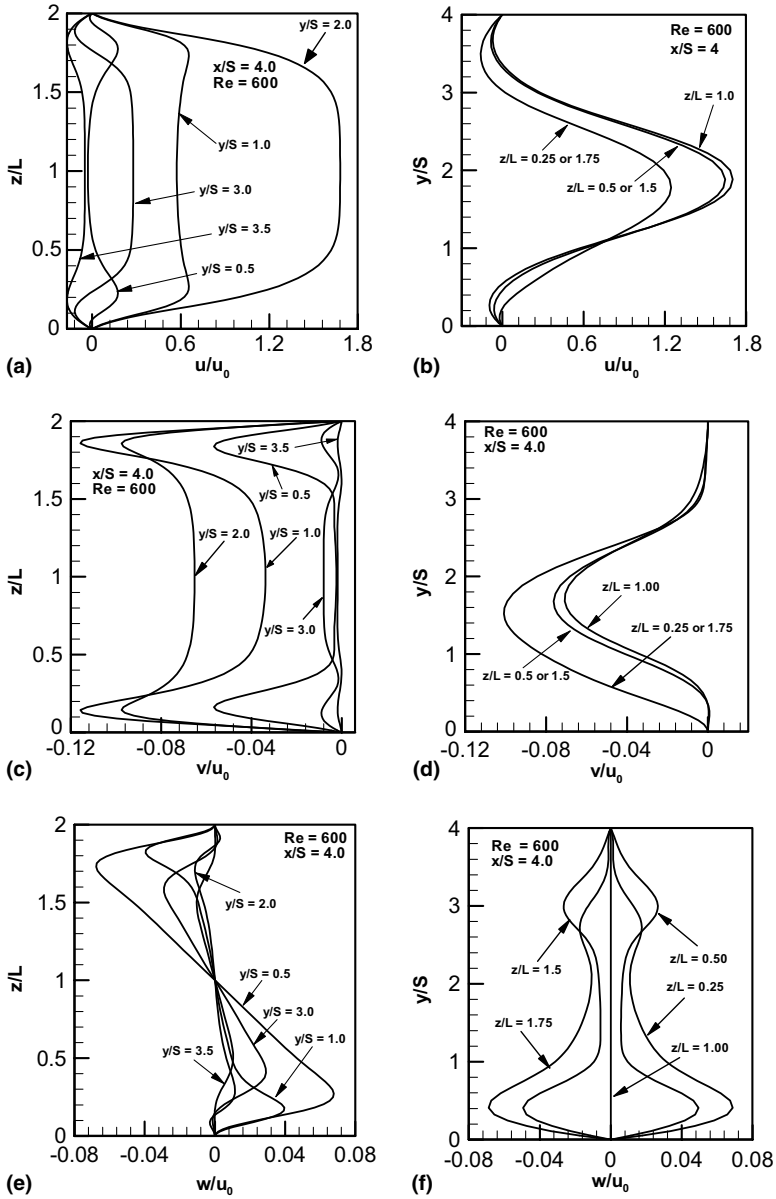

Fig. 2. Velocity distributions for $Re = 600$.

be seen in Figs. 2 and 3 for $Re = 600$. The results in these figures show that the velocity and temperature distributions are symmetric in the spanwise direction and un-symmetric in the transverse direction. As a result of the spanwise symmetry, the width of the computational domain is chosen as half of the actual width of the duct, $L = 0.04$ m, and symmetry boundary conditions are applied at the center plane of the duct, i.e. at $z = 0.04$ m, $w = 0$, and the gradient of all the other quantities with respect to z are set equal to zero. Results that were generated using this smaller domain (half width) compared exactly with the results that were generated using the full width domain.

The computational grid distribution was selected to ensure high density near all of the bounding walls and in the regions of the step where high gradients exist, in order to ensure the accuracy of the simulations. Grid independence tests were performed using eight different

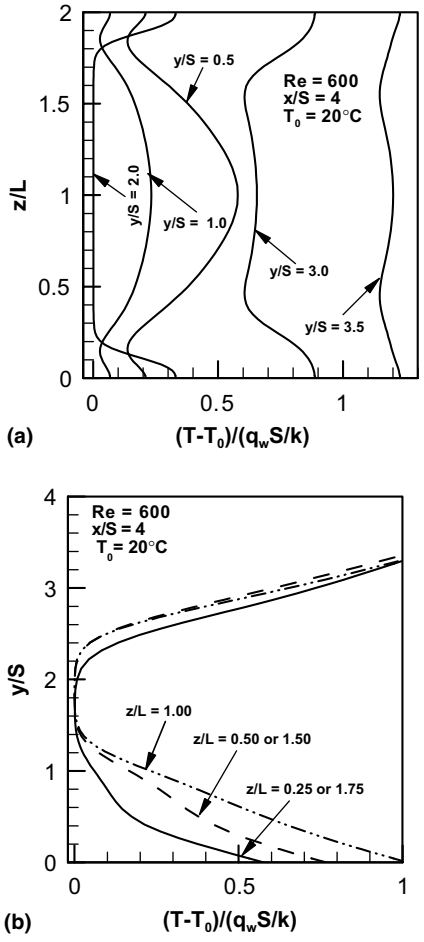

Fig. 3. Temperature distributions for $Re = 600$.

grid densities and distributions downstream of the sudden expansion for $Re = 600$. Comparisons of these results show that using a grid of $(200 \times 64 \times 50)$ downstream of the sudden expansion $(0 \leqslant x/S \leqslant 80)$ and a grid of $(20 \times 32 \times 50)$ upstream of the sudden expansion $(-2 \leqslant x/S \leqslant 0)$ for half of the duct's width $(0 \leqslant z/L \leqslant 1)$ provides a grid independent results, and this grid was used for all the results that are presented in this paper.

The use of both the steady and the transient Navier–Stokes equations for simulating the steady bifurcated flow that develops in this geometry was examined. The distributions of the resulting steady streamwise velocity component simulated by these two schemes were compared for $Re = 800$, and the excellent agreements between the results from the two simulation schemes (steady and transient) justify the use of the steady Navier–Stokes equations for simulating the steady bifurcated flow regime. Our predicted distributions for the streamwise velocity component in the same geometry as the one used in the experiment by Fearn et al. [1] compare very favorably with his published measurements, thus validating the accuracy of the simulation code.

4. Results and discussion

Simulations of the flow and heat transfer were performed for Reynolds numbers of 150, 350, 400, 450, 600, and 800 in the geometry that is presented in Fig. 1. The flow at these Reynolds numbers is laminar and steady with flow bifurcation developing for $Re > 400$, and symmetric non-bifurcated flow developing for $Re < 400$. This study will focus on presenting flow and heat transfer results in the bifurcated flow regime ($Re > 400$). The bifurcated flow that developed in our simulations resulted in stable bifurcated states where the reverse flow region that develops adjacent to the lower stepped wall is smaller than the one that develops adjacent to the upper stepped wall. Due to space limitations and due to the fact that the results are similar for different Reynolds numbers, most of the presented results are for $Re = 600$. Results for other Reynolds numbers are presented, when warranted, to illustrate the effects of the Reynolds number.

The general flow features that develop downstream from the sudden expansion are presented in Fig. 4 for $Re = 600$. A primary recirculation flow region develops adjacent to the lower stepped wall and a larger recirculation flow region develops adjacent to the upper stepped wall. A third but smaller recirculation flow region develops further downstream on the lower stepped wall but that reverse flow region exists only close to the sidewall and does not extend to the center of the duct as can be seen in Fig. 4c. A downwash and several "jet-like" flow regions develop adjacent to the sidewall. The downwash flows in a counter-clockwise swirling motion towards the lower stepped wall and into the primary reverse flow region while moving in the spanwise direction toward the center of the duct. Three "jet-like" flow impingement regions can be seen in Fig. 4a, with one on the upper stepped wall (at $x/S = 29.24$, $z/L = 0.185$) and two on the lower stepped wall (at $x/S = 5.684$, $z/L = 0.165$, and $x/S = 32.0$, $z/L = 0.039$). A reverse flow region develops in the neighborhood of each impingement region as can be seen in Fig. 4a. Streamlines at different spanwise planes are presented in Fig. 4c to demonstrate the flow behavior near the sidewall. The general flow features that develop in the region of $0.20 < z/L < 1$ (close to the center of the duct) do not change significantly, and for that reason are not represented in Fig. 4c. Similar results are available for other Reynolds numbers but are not presented due to space limitations. The locations of the "jet-like" flow impingement for $Re = 450$ on the lower stepped wall are $x/S = 7.426$, $z/L = 0.311$, and on the upper stepped wall they are at $x/S = 17.475$, $z/L = 0.346$. The locations

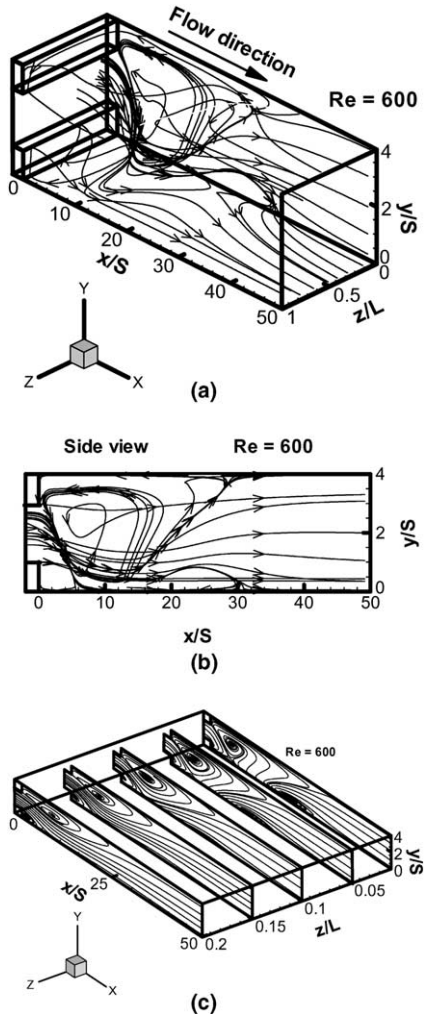

Fig. 4. Streamlines demonstrating general flow features.

of the "jet-like" flow impingement for $Re = 800$ on the lower stepped wall are $x/S = 5.403$, $z/L = 0.130$, and $x/S = 43.171$, $z/L = 0.042$, and on the upper stepped wall they are at $x/S = 38.844$, $z/L = 0.129$.

Limiting streamlines adjacent to the upper stepped wall, lower stepped wall and sidewall are presented in Fig. 5 to illustrate additional flow features downstream of the sudden expansion. There are two "jet-like" flow impingement locations that appear on the lower stepped wall and one that appear on the upper stepped wall as was discussed in the previous paragraph but can be seen more clearly in this figure for $Re = 600$. At these points, the streamwise and the spanwise components of the wall shear stress, $(\mu\partial u/\partial y)$ and $(\mu\partial w/\partial y)$, are zero. The impingement point acts as a source from which streamlines originate. Some of these streamlines flow downstream and later reverse their direction while moving towards the sidewall and in that process a reverse flow

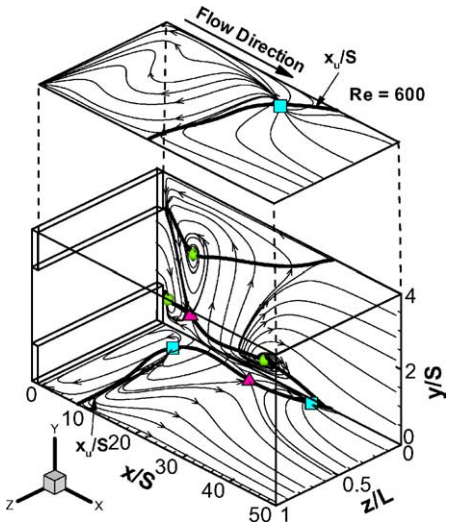

Fig. 5. Limiting streamlines adjacent to the bounding walls ((▲) saddle point; (■) "jet-impingement"; and (●) focal point locations).

region develops adjacent to the sidewall as can be seen in Fig. 5. The saddle points that develop on the lower stepped wall and on the sidewall represent critical points in the flow where two streamlines approach that point from different angles and rebound to form the boundaries of four different flow regions around the saddle point. The three Focal points that develop on the sidewall represent critical points in the flow where infinite number of streamlines spiral around. Two of these focal points are attractive and one is repelling. The repelling focal point is the one located farthest downstream from the sudden expansion as shown in Fig. 5. The bold solid lines that are shown in Fig. 5 represent the locations where the streamwise component of the wall shear stress $(\mu\partial u/\partial y)$ is zero (x_u-line) for the two stepped walls and $(\mu\partial u/\partial z)$ is zero for the sidewall.

Distributions of the x_u-lines are presented in Fig. 6 for both $y/S = 0.01$ and 3.99 (the two stepped walls). The locations of the saddle points and the "jet-like" flow impingement points are included on this figure. This definition (x_u-line) is commonly used to identify the reattachment length in two-dimensional separated-reattached flow. The x_u-line moves further downstream as the Reynolds number increases and its maximum develops at the sidewall for both the upper and the lower stepped walls. A minimum develops in the x_u-line on the lower stepped wall near the sidewall and that minimum moves closer to the sidewall and closer to the step as the Reynolds number increases, i.e. behaving in a similar fashion as to the impingement location of the "jet-like" flow. It is interesting to note that in the center region of the duct $0.8 < z/L < 1.0$ the effect of the Reynolds number on the x_u-line for the lower wall is negligible. Two

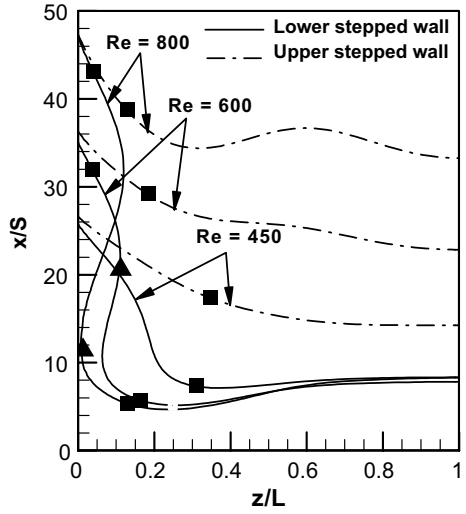

Fig. 6. Distributions of x_u lines adjacent to the two stepped walls ($y/S = 0.01$ and 3.99) ((▲) saddle point and (■) "jet-impingement" locations).

"jet-like" flow impingement regions develop on the lower stepped wall for $Re = 600$ and 800, but only one develops for $Re = 450$.

The limiting streamlines that are presented in Fig. 5 are also used to identify the outer boundary of the recirculation regions (x_b-lines) that develop adjacent to the bounding walls. These boundary lines, (x_b-lines) are determined by the criterion that streamlines on both sides of these boundary lines move in opposite directions: streamlines upstream from this line flow upstream toward the step, and streamlines downstream from this line flow downstream and away from the step. Distributions of the x_b-lines on the planes of $y/S = 0.01$ and 3.99 adjacent to the two stepped walls are presented in Fig. 7. The x_b-line differs from the x_u-line for three-dimensional flow (especially near the sidewall), but they are identical to each other for two-dimensional flow (i.e. at the center of a duct with large aspect ratio). The x_b-lines on the upper stepped wall move further downstream from the step as the Reynolds number increases. It is interesting, however, to note that in the center region of the duct ($0.8 < z/L < 1.0$) the effect of the Reynolds number on the x_b-line for the lower stepped wall is negligible, but near the sidewall the x_b-lines on the lower stepped wall move upstream or closer to the step as the Reynolds

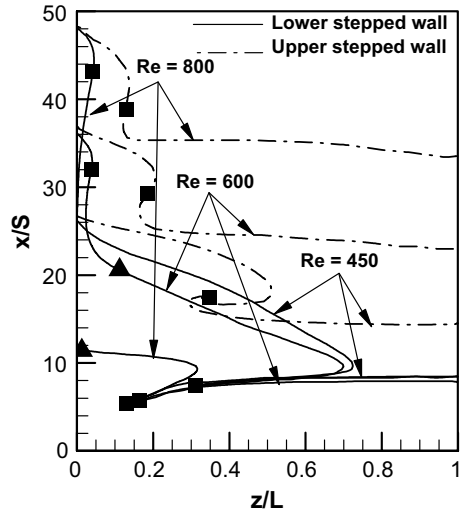

Fig. 7. Distributions of x_b-lines adjacent to the two stepped walls ($y/S = 0.01$ and 3.99) ((▲) saddle point and (■) "jet-impingement" locations).

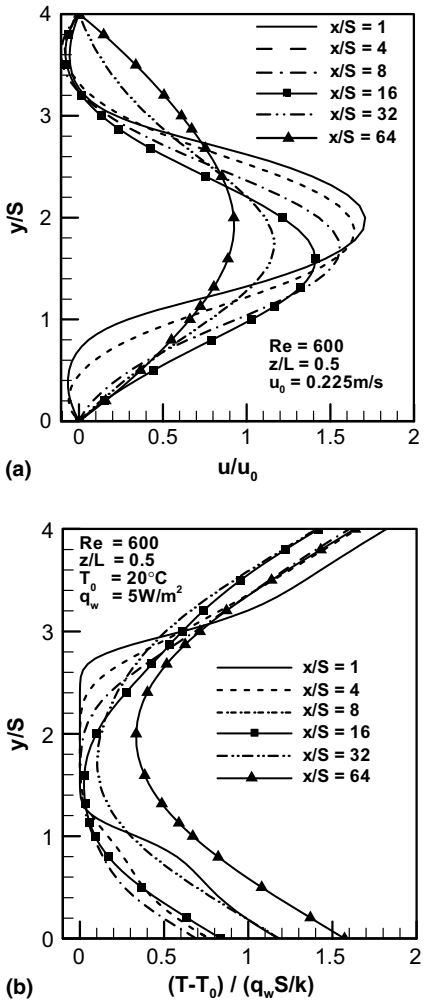

Fig. 8. Transverse distributions of the (a) streamwise velocity component and (b) temperature at different streamwise locations.

number increases. Two separated reverse flow regions develop for $Re = 800$, but only one develop for $Re = 450$ and 600.

Transverse distributions of velocity and temperature at different streamwise locations are presented in Fig. 8 for $Re = 600$. These figures illustrate the non-symmetric behaviors that develop in these distributions inside this symmetric geometry. The non-symmetric behaviors that appear in the bifurcated flow region disappear in the fully developed flow. In the bifurcated flow region the distribution of streamwise velocity component tilts towards the wall that has the smaller reverse flow region (the lower stepped wall in this case). This asymmetric flow behavior leads to a lower fluid temperature in that region, and to asymmetric temperature distribution. These features influence the magnitude and the distribution of the Nusselt number on the stepped walls.

Distributions of the velocity and temperature fields are presented in Fig. 9 for those streamwise intersectional planes where the "jet-like" flow impinges on the lower and upper stepped walls. The velocity vectors in this figure represent the sum of the transverse and spanwise velocity components. The wall temperature decreases and the spanwise velocity component increases in the "jet-like" flow impingement regions. It is interesting to note that the lower stepped wall is at a lower temperature than the upper stepped wall at $x/S = 5.684$ (where the "jet like" flow impinges on the lower wall), and also at $x/S = 29.24$ (where the "jet-like" flow impinges on the upper wall).

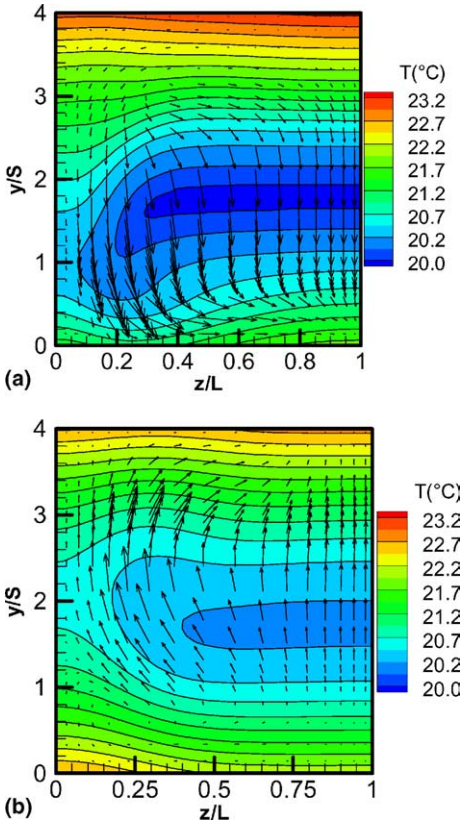

Fig. 9. Velocity and temperature fields for $Re = 600$ at: (a) $x/S = 5.684$ and (b) $x/S = 29.24$.

Results in Fig. 10 represent the velocity field on a plane adjacent to the lower stepped wall ($y/S = 0.01$). The velocity vectors in this figure represent the sum of the spanwise and streamwise velocity components and the color in this figure represents the magnitude of the transverse (normal) velocity component. The locations where "jet-like" flow impinges on the stepped wall and the location where the Nusselt number is a maximum are identified in this figure. It can be seen that the location of the maximum Nusselt number does not coincides with the location where the "jet-like" flow impinges on this stepped wall. The x_u-line is also presented in this figure, and it passes through a region where the transverse velocity component is positive near the sidewall, thus indicating that the x_u-line in that region of the flow does not represent a reattachment of the separating shear layer on the stepped wall. It is also interesting to note that the location where the maximum Nusselt number develops on the stepped wall is in the same region where the magnitude of the transverse velocity component is a maximum.

Results in Fig. 11 represent the velocity field on a plane adjacent to the upper stepped wall ($y/S = 3.99$). The location where "jet-like" flow impinges on this stepped wall and the location where the Nusselt number is a maximum are identified in this figure. The location of the maximum Nusselt number is significantly upstream from the "jet-like" impingement location, inside the primary recirculation flow region. The x_u-line is also presented in this figure, and it passes through a region where the transverse velocity component is positive (near the sidewall), thus indicating that the x_u-line in

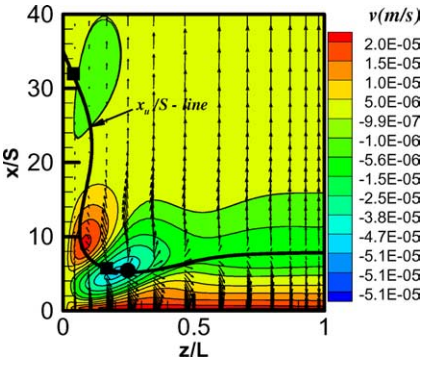

Fig. 10. Velocity field on a y-plane adjacent to the lower stepped wall ($y/S = 0.01$), $Re = 600$ ((●) maximum Nusselt number; (■) "jet-impingements" locations).

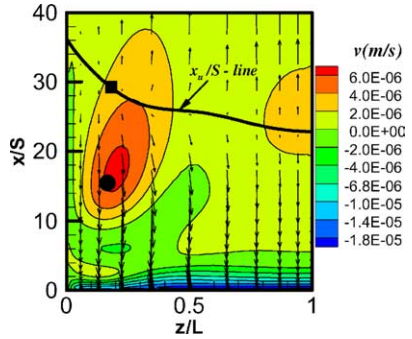

Fig. 11. Velocity field on a y-plane adjacent to the upper stepped wall ($y/S = 3.99$), $Re = 600$ ((●) maximum Nusselt number; (■) "jet-impingement" locations).

that region of the flow does not represent a reattachment of the separating shear layer. The maximum Nusselt number develops on this stepped wall is in the same general region where the magnitude of the transverse velocity component incident on that wall is a maximum. Results in Fig. 12 represent the velocity field on a plane adjacent to the sidewall ($z/L = 0.01$). The velocity vectors in this figure represent the sum of the streamwise and transverse velocity components and the color represents the magnitude of the spanwise velocity component. The downwash that develops at the corner of the step can be seen in this figure. The locations of the saddle point and the Focal points that develop on this plane along with the line that locates the minimum temperature on this plane are identified in this figure. It is interesting to note that the minimum sidewall temperature develops in the general region where the magnitude of the spanwise velocity component (velocity normal to the sidewall) is a maximum.

Nusselt number ($Nu = q_w S/k(T_w - T_0)$) distributions on the two stepped walls are presented in Figs. 13 and 14 for $Re = 600$. The results show that the maximum Nusselt number develops near the sidewall and not at

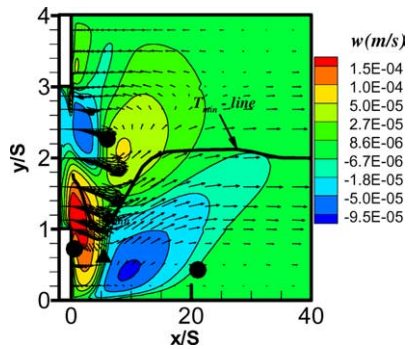

Fig. 12. Velocity field on a z-plane adjacent to the sidewall ($z/L = 0.01$), $Re = 600$ ((▲) saddle point; (●) focal point locations).

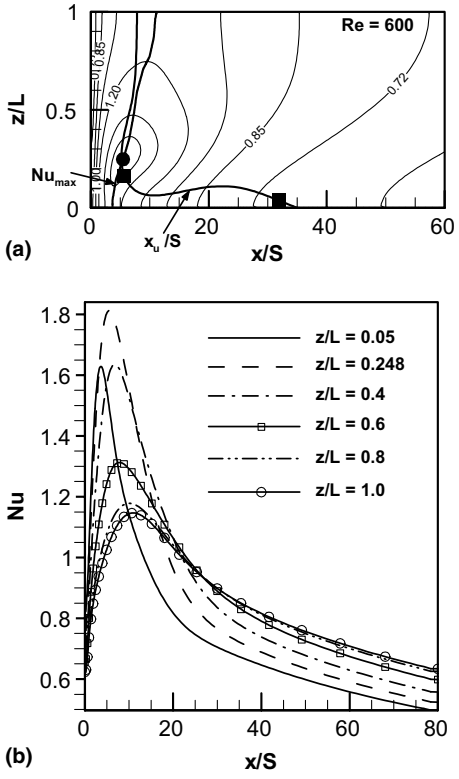

Fig. 13. Nusselt number distribution on the lower stepped wall ($y/S = 0$) ((●) maximum Nusselt number; (■) "jet-impingement" locations).

the center of the duct. The maximum Nusselt number that develops on the lower stepped wall (the wall with the smaller recirculation flow region) is higher than the maximum Nusselt number that develops on the upper stepped wall (the wall with the larger recirculation flow region). Similarly the location of that maximum on the lower stepped wall is significantly closer to the sudden expansion than the one on the upper stepped wall. The spanwise distributions of the Nu_{max}-line (locations where the Nusselt number is a maximum), and the x_u-line are presented in these figures. The Nu_{max}-line moves further downstream from the step and the maximum Nusselt number moves closer to the sidewall as the Reynolds number increases. The maximum Nusselt numbers on the lower stepped wall are 1.191 (at $x/S = 4.785$, $z/L = 0.271$), 1.813 (at $x/S = 5.45$, $z/L = 0.248$) and 2.332 (at $x/S = 5.728$, $z/L = 0.248$) for $Re = 450$, 600 and 800, and on the upper stepped wall they are 0.763 (at $x/S = 11.377$, $z/L = 0.271$), 0.804 (at $x/S = 15.508$, $z/L = 0.167$) and 0.885 (at $x/S = 27.0$, $z/L = 0.186$), respectively. The magnitude of the maximum Nusselt number that develops on the lower stepped wall is larger than the magnitude of the Nusselt number that develops on the upper stepped wall. Similarly, the distance from

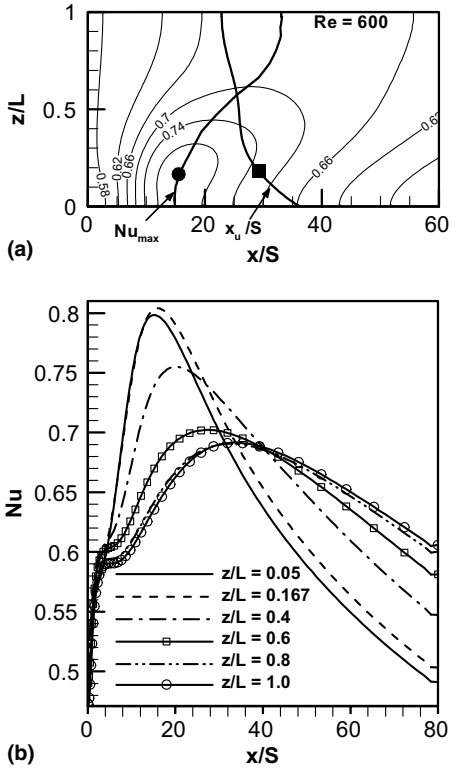

Fig. 14. Nusselt number distribution on the upper stepped wall ($y/S = 4$) ((●) maximum Nusselt number; (■) "jet-impingement" locations).

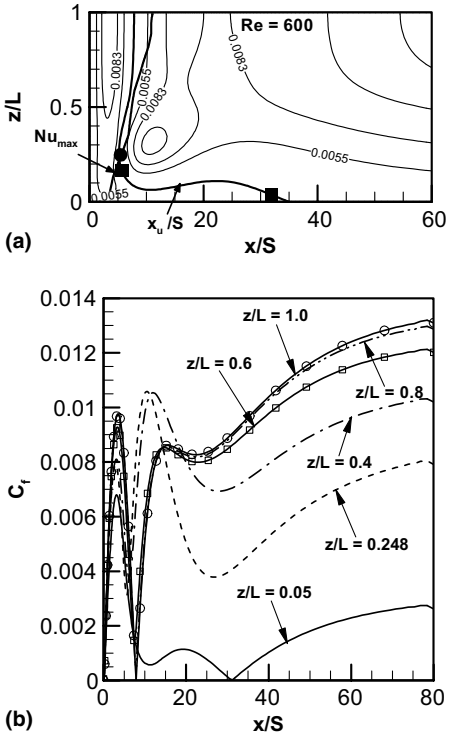

Fig. 15. Friction coefficient distribution on the lower stepped wall ($y/S = 0$) for $Re = 600$ ((●) maximum Nusselt number; (■) "jet-impingement" locations).

the sudden expansion where that maximum develops on the upper stepped wall is more than twice the distance that the maximum develops on the lower stepped wall. The results in Figs. 13b and 14b illustrate the rapid increase of the Nusselt number to a peak value after the sudden expansion, and that peak develops near the sidewall. The Nusselt number gradually decreases after the peak point as the flow approaches the fully developed region where the location of the maximum Nusselt number gradually moves from the sidewall toward the center of the duct as the streamwise distance from the sudden expansion continues to increase. The second "jet-like" flow that impinges on the lower stepped wall is relatively small in magnitude and for that reason it does not appear to affect significantly the Nusselt number distribution in that region. It should be noted that the Nusselt number is inversely proportional to the wall temperature.

Distributions of the friction coefficient on the two stepped walls are presented in Figs. 15 and 16 for $Re = 600$. These results illustrate that the friction coefficient increases rapidly after the sudden expansion and a maximum develops inside the primary recirculating flow region (upstream of the x_u-line). The location of that maximum is in the center of the duct for the lower stepped wall and closer to the sidewall for the upper stepped wall. The location of the maximum in that region moves farther downstream from the sudden expansion as the Reynolds number increases. The magnitude of the friction coefficient then decreases rapidly to a minimum, and the spanwise locations of that minimum are designated by the x_u-lines that are presented in these figures. The friction coefficient increases rapidly after the x_u-lines, developing a local peak near the sidewall on the lower stepped wall, and a maximum at the center of the duct in the fully developed region. The Nu_{max}-line is presented in these figures to illustrate its relative location as compared with the x_u-line.

Temperature distributions on the sidewall are presented in Fig. 17 for $Re = 600$. The lack of symmetry relative to the center height of the sidewall near the sudden expansion (in the bifurcated flow region) can be seen in these figures. The temperature distribution is skewed towards the lower stepped wall (the wall with the smaller recirculating flow region), thus creating a lower temperature in that region of the flow. A line identifying the location where the wall temperature is a minimum is included in this figure. The wall temperature increases as the distance from the duct's center increases due to its

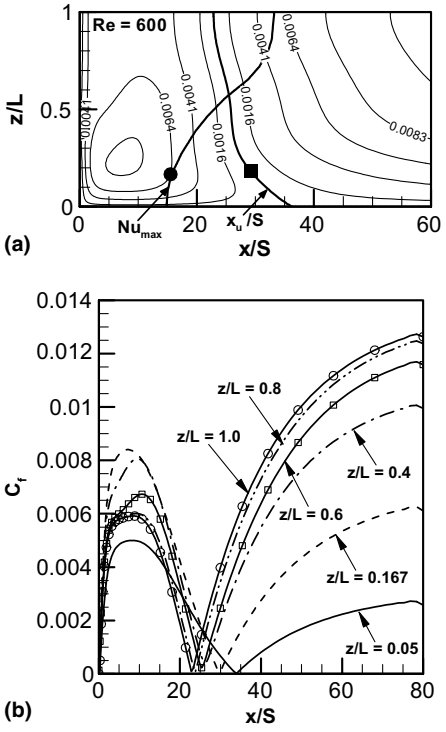

Fig. 16. Friction coefficient distribution on the upper stepped wall ($y/S = 4$) for $Re = 600$ ((●) maximum Nusselt number; (■) "jet-impingement" locations).

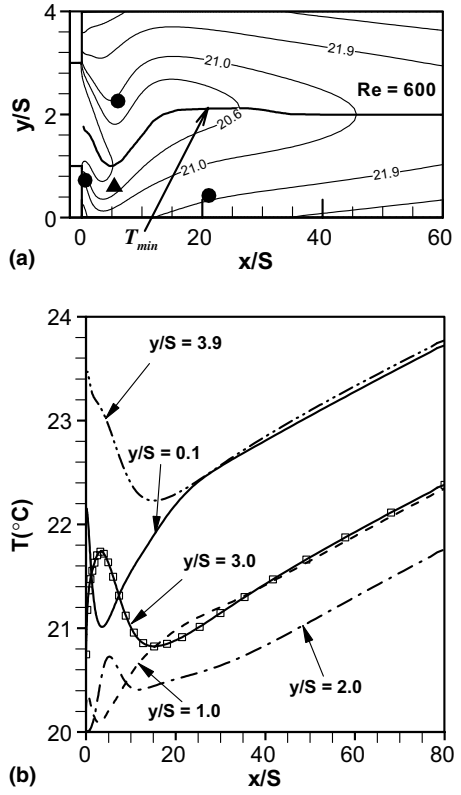

Fig. 17. Sidewall temperature distribution ($z/L = 0$) for $Re = 600$ ((▲) saddle point; (●) "focal point" locations).

proximity to the heated stepped walls. Similarly the temperature increases as the distance from the sudden expansion increases due to the added energy from the heated bounding walls. Symmetry develops in the sidewall temperature distribution as the fully developed flow region is approached. Distributions of the friction coefficient on the sidewall are presented in Fig. 18 for $Re = 600$. Several peaks develop in this distribution and their magnitude decreases as the Reynolds number increases. The local peaks that develop in that distribution and its general streamwise behavior can be seen in Fig. 18b.

5. Conclusions

Simulations of three-dimensional laminar forced convection in plane symmetric sudden expansion in rectangular duct with an expansion ratio of two and downstream aspect ratio of two are presented for $Re = 450$, 600 and 800. The bifurcated flow for this Reynolds number range is laminar, steady and asymmetric in the transverse directions, but symmetric relative to the center width of the duct in the spanwise direction. A strong downwash develops at the corner of the step near the sidewall causing the reverse flow region that develops adjacent to the lower stepped wall to be smaller than the one that develops adjacent to the upper stepped wall. The "jet-like" flow that impinges on the lower stepped wall originates from the top corner of the inlet section, but that flow develops a reversed spiral flow region adjacent to the sidewall before its impingement on the lower stepped wall. The maximum Nusselt number that occurs on the lower stepped wall is larger than the one that develops on the upper stepped walls. The maximum Nusselt number develops near the sidewall and not at the center of the duct. Its location on the lower stepped wall is closer to the sudden expansion than its location on the upper stepped wall. The maximum Nusselt numbers on the stepped walls do not develop at the impingement location of the "jet-like" flow, but in the region where the magnitude of the transverse velocity component incident on the wall is a maximum. The second "jet-like" flow impingement on the lower stepped walls has little effect on the Nusselt number distribution due to its relatively very small magnitude. The friction coefficient is slightly higher on the lower stepped wall in comparison with the upper stepped wall in the bifurcated flow region. The results also reveal that the locations where the streamwise component of wall shear stress is zero on the stepped walls (x_u-line) do not coincide with

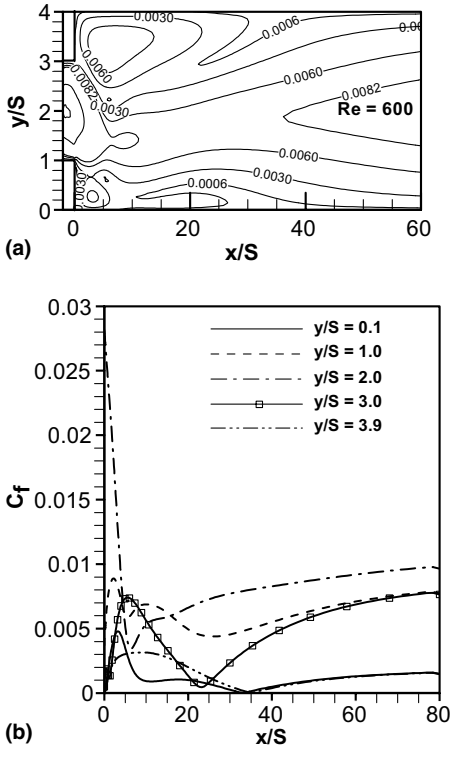

Fig. 18. Friction coefficient distributions on the sidewall ($z/L = 0$) for $Re = 600$.

the outer edge of the primary recirculation flow region (x_b-lines) near the sidewalls.

Acknowledgement

This work was supported in part by a DOE-Basic Energy Sciences Grant No. DE-FG02-03ER46067.

References

[1] R.M. Fearn, T. Mullin, K.A. Cliffe, Nonlinear flow phenomena in a symmetric sudden expansion, J. Fluid Mech. 211 (1990) 595–608.
[2] F. Durst, A. Melling, J.H. Whitelaw, Low Reynolds number flow over a plane symmetric sudden expansion, J. Fluid Mech. 64 (1974) 111–128.
[3] F. Durst, J.C.F. Pereira, C. Tropea, The plane symmetric sudden-expansion flow at low Reynolds numbers, J. Fluid Mech. 248 (1993) 567–581.
[4] W. Cherdron, F. Durst, J.H. Whitelaw, Asymmetric flows and instabilities in symmetric ducts with sudden expansions, J. Fluid Mech. 84 (1978) 13–31.
[5] T. Hawa, Z. Rusak, The dynamics of a laminar flow in a symmetric channel with a sudden expansion, J. Fluid Mech. 436 (2001) 283–320.
[6] F. Battaglia, S.J. Travener, A.K. Kulkarni, C.L. Merkle, Bifurcation of low Reynolds number flows in symmetric channels, AIAA J 35 (1997) 99–105.
[7] D. Drikakis, Bifurcation phenomena in incompressible sudden expansion flows, Phys. Fluids 9 (1997) 76–87.
[8] S. Patel, D. Drikakis, Numerical effects on the prediction of flow instabilities in channels with sudden-expansions, in: Proceedings of IMECE'03, ASME-IMECE2003-55616, Washington, DC, 2003, pp. 16-21.
[9] T.P. Chiang, T.W.H. Sheu, S.K. Wang, Side wall effects on the structure of laminar flow over a plane-symmetric sudden expansion, Comput. Fluids 29 (2000) 467–492.
[10] E. Schreck, M. Schafer, Numerical study of bifurcation in three-dimensional sudden channel expansions, Comput. Fluids 29 (2000) 583–593.
[11] Y.Y. Tsui, S.J. Shu, Effects of buoyancy and orientation on the flow in a duct with a double-step expansion, Int. J. Heat Mass Transfer 41 (1998) 2687–2695.
[12] J.H. Nie, B.F. Armaly, Three-dimensional forced convection in plane symmetric sudden expansion, ASME J. Heat Transfer 126 (2004) 836–839.
[13] R.K Shah, A.L. London, Laminar Forced Convection in Ducts, Academic Press, New York, 1978, pp. 196–198.